Supplementary Information

Breaking the trade-off with ordered nanochannels for high-effective osmotic energy conversion

Jiale Song [a], Zhiliang Han [a], Zhou Zhou [a], Shengming Zhang [a], Minghao Zhang [b,*], Xiangyang Qu [a], Xiangguo Lv [c,*], Shiyan Chen [a,*], Huaping Wang [a]

[a] *State Key Laboratory of Advanced Fiber Materials, College of Materials Science and Engineering, Donghua University, Shanghai 201620, PR China;*

[b] *Faculty of Materials Technology, Shanghai Institute of Technology, Shanghai 201418, China;*

[c] *Department of Urology, Renji Hospital, School of Medicine, Shanghai Jiao Tong University, Shanghai, 200127, PR China*

Corresponding Author:

Minghao Zhang, email: mhzhang@sit.edu.cn

Xiangguo Lv, email:chnlvsc@163.com

Shiyan Chen, email: chensy@dhu.edu.cn

Table of content

Experimental methods and characterizations

Chemicals:

BC was prepared in our laboratory by culturing Gluconacetobacter xylinus. XLS, potassium chloride (KCl), sodium chloride (NaCl), sodium hypochlorite (NaClO)，TEMPO (2,2,6,6-tetramethylpiperidine-1-oxyl radical), sodium bromide (NaBr), NaOH, HCl and were all purchased from Sinopharm Chemical Reagent Beijing Co. Ltd. Plastic box was purchased from Suining Kexin Instrument and Meter Business Department. An epoxy resin (#E−44 resin and 650 curing agent) was used to assemble the units. Ultrapure deionized water (18 MΩ cm) was used to prepare salt solution of different concentrations. The PBS buffer was purchased from Hunan Bikeman Holding Co., Ltd., and the artificial urine was purchased from Guangzhou Deli Chemical Co., Ltd. L929 mouse fibroblasts, fetal bovine serum, penicillin, streptomycin, basal medium, trypsin, Cell Counting Kit-8, and Calcein AM/PI cell dual-staining reagent were all purchased from Nanjing Hong'an Biotechnology Co., Ltd. The artificial urine was purchased from Guangzhou Deli Chemical Co., Ltd.

Fabrication of X-NBC composite membranes:

The BC membrane was processed into a fibrous slurry by high-shear homogenization technique. Based on previous studies, the slurry was subjected to TEMPO oxidation reaction to produce negatively charged bacterial cellulose (NBC) nanofibers. Next, the XLS dispersion was mixed with the NBC dispersion (both at a concentration of 1 mg/mL) in different ratios (0.25:1, 0.5:1, 1:1, and 5:1). The mixed suspension (total 20 mL) was filtered by vacuum filtration onto a filtration membrane. After the filtration was completed, the membrane was dried naturally at room temperature and can subsequently be easily peeled off.

Characterization:

We employed an electrochemical workstation (CHI 660) to examine the ion

transport characteristics of the individual power unit, utilizing Ag/AgCl electrode to test the *I-V* response. Under various concentration gradients, the scanning voltage range was set from −0.2 V to 0.2 V, with a step voltage of 0.01 V. For ionic conductivity tests, the chamber was filled with the same KCl concentration, spanning from 10^{-6} M to 10^{0} M. The *I-T* curve had a scanning duration of 10^{7} s with a sampling interval of 0.1 s. The open-circuit potential test (OCPT) curve was utilized to measure the voltage variations after multiple power units were connected in series, with a scanning time over 30 h and a sampling interval of 0.1 s. For *EIS* testing at 10^{-3} M, the high-frequency parameter was set at 10^{6} Hz, and the low-frequency parameter was 0.1 Hz.

After exposing X-NBC and commercial BC membranes to ultraviolet (UV) light for 24 h, they were placed in a 48−well plate for cell seeding. Fibroblasts (L929) were then cultured on these membranes at a concentration of 10^{5} cells per mL for a period of 48 h at 37 °C. Following a 30 min staining process with calcein-AM and propidium iodide (PI), the cells were examined using a fluorescence microscope.

For assessing cell viability, the sterilized X-NBC and commercial BC membranes were positioned in a 96-well plate, and L929 cells were inoculated at a density of 10^{5} cells per mL for a cultivation period of 2 to 3 d. Subsequently, a 10% solution of Cell Counting Kit-8 (CCK-8) was added. The absorbance of the culture medium was measured at 450 nm after a 90 min incubation period. The cell survival rate was calculated using the formula: Cell survival rate = $(OD_{X\text{-}NBC}–OD_0)/(OD_{BC}–OD_0)$, where $OD_{X\text{-}NBC}$ represents the optical density of the X-NBC membranes, OD_{BC} represents the optical density of the commercial BC membranes, and OD_0 represents the optical density of the well plate culture medium without cells.

The surface and cross-sectional structures of the membranes were characterized and photographed by energy dispersive spectroscopy (EDS) using a field emission scanning electron microscope (SEM, Hitachi SU8010). Flourier transform infrared spectrometer (Nicolet 8700, USA) characterized the surface chemical groups of BC, NBC and X-NBC membranes in the wavelength range of 500−4000 cm^{-1}. XRD of XLS

powders, NBC and X-NBC membranes were measured on an Andon Paar (Dynamic 500) with a scanning range of 3° to 60°. The Zeta potential of 0.2 mg mL^{-1} dispersion at pH = 7 was tested using a nanoparticle size and zeta potential analyzer (Anton paar Litersizer 500). The samples were irradiated with visible light (400−780 nm) and UV light (365 nm) for 10 minutes on a contact angle tester (JC2000D2A). At room temperature, 4 μL of water (3 different sites) was dropped on the sample surface with the contact angle meter, and the contact angle was read after 10 seconds of standing, and the average of three measurements was taken. Rheological characterization of hydrogels was carried out by using a rheometer (MCR302, Anton Paar). Perform amplitude scan and time scan tests under the condition of γ = 1 %. Specific surface area and pore size distribution of membranes were estimated using N_2 adsorption isotherms obtained from (Autosorb iQ). Prior to analysis, samples were subjected to degassing at 120 °C for 10 h.

Formula Calculation

The Debye length λ_d in electrolyte solution:

$$\frac{1}{\lambda_d}\sim\sqrt{\lambda_B I}=\sqrt{\frac{e^2}{\varepsilon\varepsilon_0 K_B T}\sum_i c_i z_i^2}\#(S1)$$

where e is the electron charge, K_B is the Boltzmann constant, T is the temperature, λ_B is Bjerrum length, c_i is the ion concentration, z_i is the charge valence of each species. The Debye length was about 9.6 nm in an aqueous KCl solution with a concentration of 0.001 M.

The surface charge density value:

$$\sigma=\frac{\varepsilon\varepsilon_0\zeta}{\lambda_d}\#(S2)$$

where ε is the dielectric constant of pure water, ε_0 is the permittivity of vacuum, ζ is the zeta potential.

The Pmax value:

$$P_{max}=\frac{I_{SC}V_{OC}}{4S}\#(S3)$$

where *Isc* is short-circuit current, *Voc* is open-circuit voltage, and *S* is the test area of the membrane.

The cation transference number (t^+):

$$t^+=\frac{1}{2}\left(1+\frac{E_{diff}}{\frac{RT}{ZF}\ln\left(\frac{\gamma_H c_H}{\gamma_L c_L}\right)}\right)\#(S4)$$

where *R, T, z, F,* γ, c_H, and c_L represent the gas constant (8.3145 J mol^{-1} K^{-1}), temperature (298 K), charge valence, Faraday constant (96485.34 C mol^{-1}), ion activity coefficient, high ion concentration, and low ion concentration, respectively.[1]

Modified Donnan equilibrium analysis of geometric compensation:

Donnan equilibrium analysis:

$$E_{mem} = E_{Don}^{dilute} + E_{diff}^{membrane} + E_{Don}^{concentrated} \#(S5)$$

At each membrane/solution interface, the intramembrane cation and anion concentrations satisfy the Donnan equilibrium:

$$c_{+}^{mem} = \frac{X_v + \sqrt{X_v^2 + 4c^2}}{2} \#(S6a)$$

$$c_{-}^{mem} = \frac{-X_v + \sqrt{X_v^2 + 4c^2}}{2} \#(S6b)$$

where c_L is the external electrolyte concentration at the dilute side.

For a slit-shaped nanochannel with height h and surface charge density σ, the volumetric fixed charge concentration is:

$$X_v = \frac{2\sigma}{Fh} \#(S7)$$

where F = 96485 C mol^{-1} is the Faraday constant. This quantity has the same units as bulk electrolyte concentration and enters the Donnan equilibrium directly. Note that X_V is equivalent to the volume charge density $X = 2\sigma/(FRp)$ used in cylindrical pore models, adapted here for slit geometry.[2]

Assuming that the cation and anion mobilities are approximately equal (in a KCl system), the cation mobility is:

$$t^+ = \frac{C_{+}^{mem}}{C_{+}^{mem} + C_{-}^{mem}} = \frac{X_v + \sqrt{X_V^2 + 4c^2}}{2\sqrt{X_V^2 + 4c^2}} \#(S8)$$

Simplified to:

$$t^+ = \frac{1}{2} + \frac{\xi}{2\sqrt{\xi^2 + 4}}, \xi = \frac{X_v}{c} \#(S9)$$

The electrochemical energy conversion efficiency (η).

$$\alpha = \frac{V_{meas}}{V_{thea}} \times 100\% \#(S10)$$

$$V_{thea} = N\frac{RT}{ZF}\ln\left(\frac{\alpha_c}{\alpha_d}\right)\#(S11)$$

where V_{meas} is the measured membrane potential, V_{thea} is the theoretical membrane potential assuming 100% membrane permeability, N is the number of membranes, R is the universal gas constant, T is the absolute temperature (K), Z is the electrochemical valence, F is Faraday's constant, a_c is the activity of the highly concentrated solution, and a_d is the activity of the dilute concentrated solution [3].

$$\eta_{maxw} = \frac{\alpha^2}{2}\#(S12)$$

Figure and Table

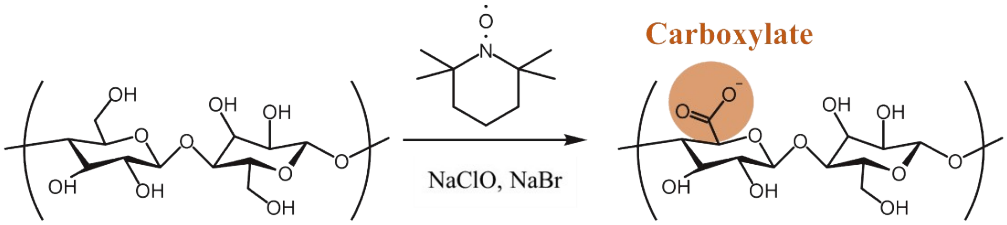

Fig. S1. TEMPO oxidized cellulose reaction.

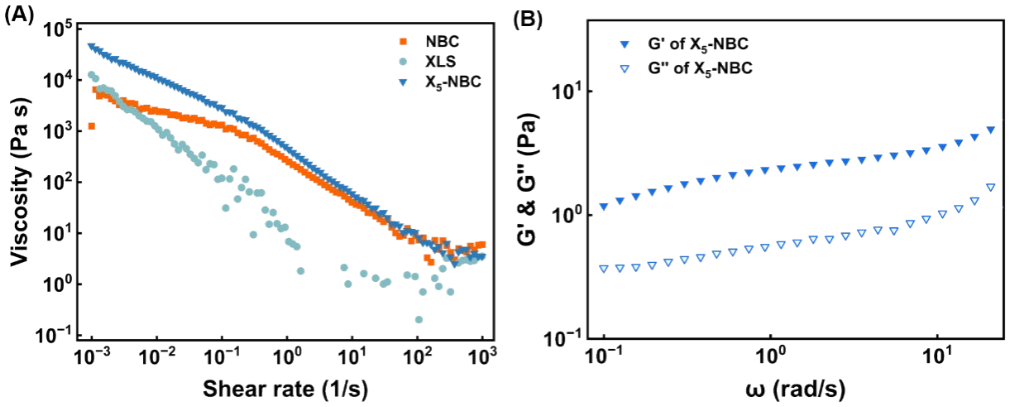

Fig. S2. (A) Shear viscosity of the NBC, XLS, and X_5-NBC dispersion solution. (B) Frequency dependence of G' and G" of X_5-NBC.

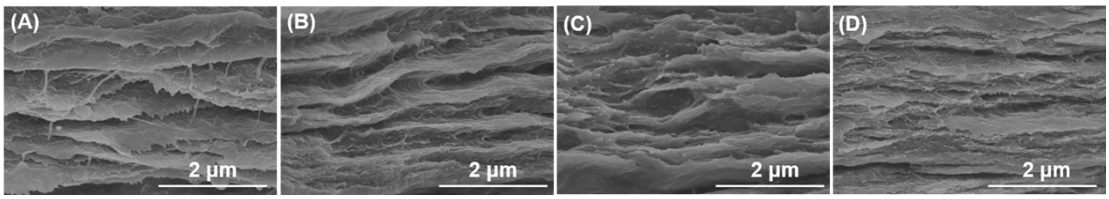

Fig. S3. Cross-sectional SEM images of (A) NBC, (B) $X_{0.25}$-NBC, (C) $X_{0.5}$-NBC, and (D) X_1-NBC.

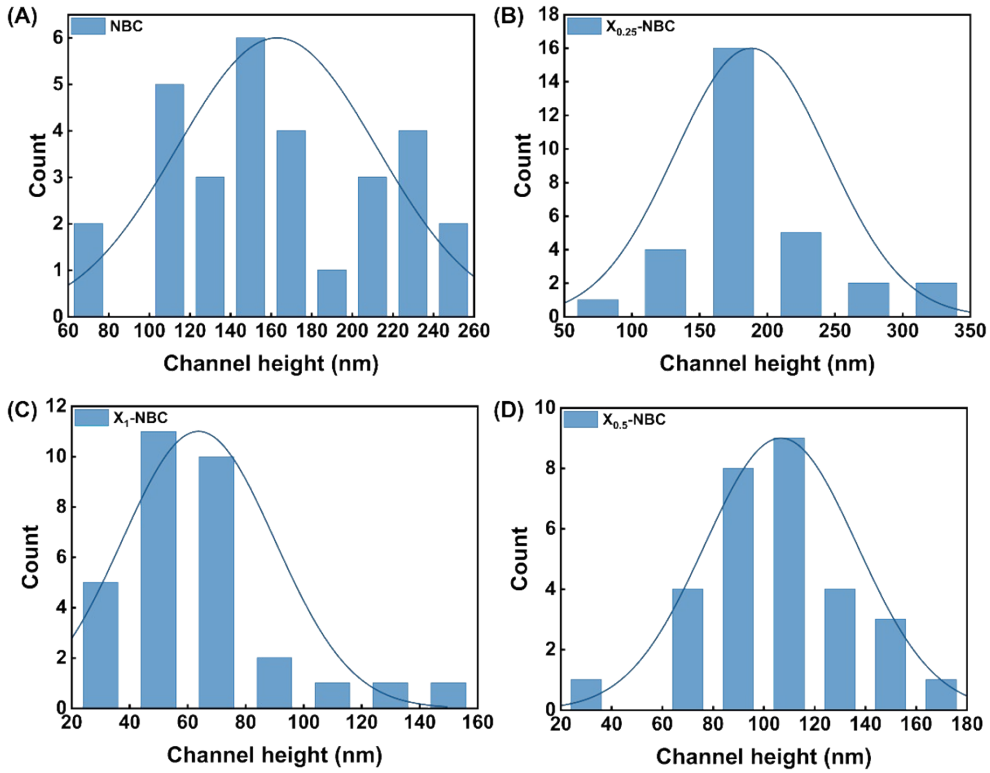

Fig. S4. Channel height distribution of (A) NBC (B) $X_{0.25}$-NBC, (C) $X_{0.5}$-NBC, (D) X_1-NBC.

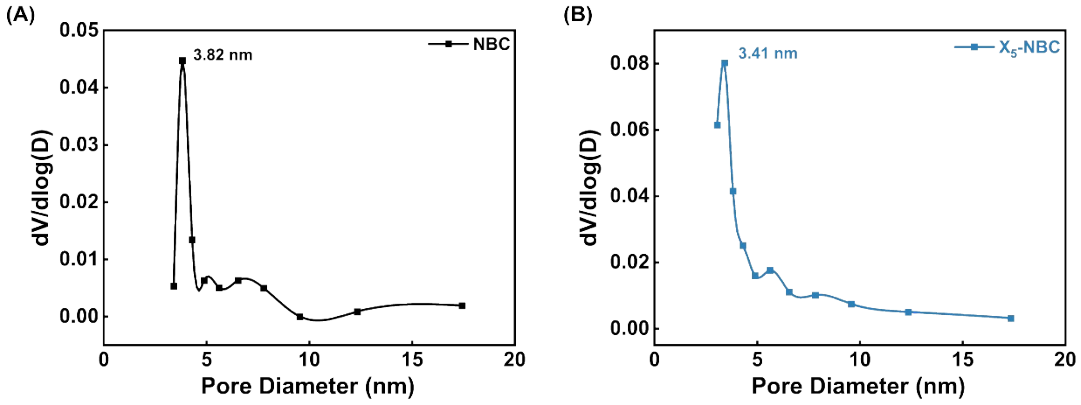

Fig. S5. Pore size distribution curves of (A) NBC and (B) X_5-NBC measured using BET analysis.

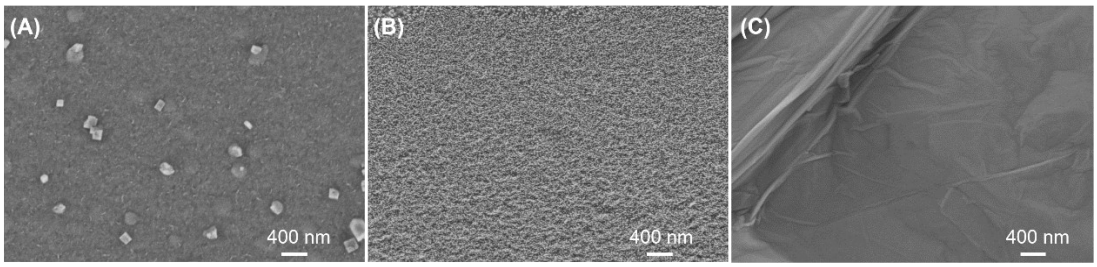

Fig. S6. Surface SEM images of (A) XLG, (B) XLS, and (C) GO dispersion.

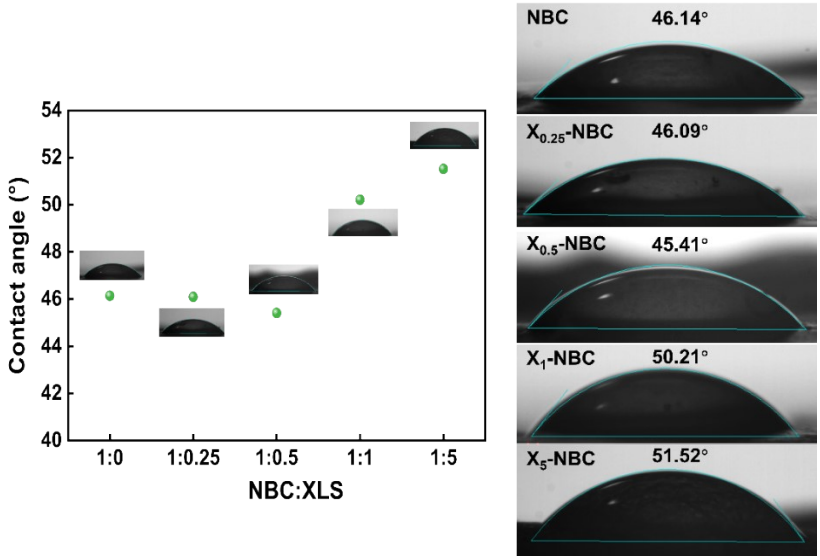

Fig. S7. Contact angle testing of X-NBC membranes with different XLS contents.

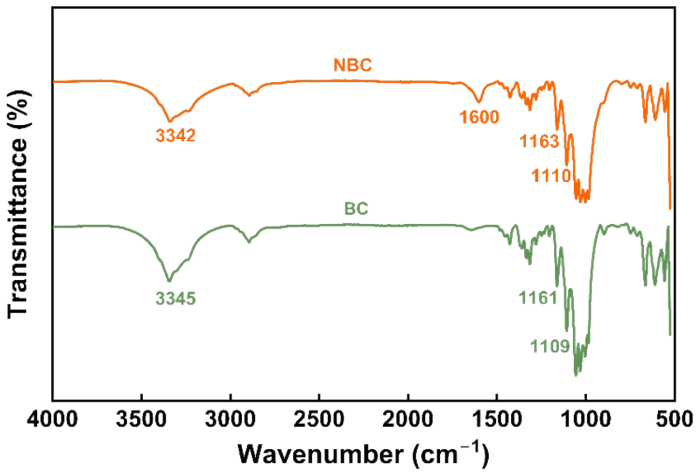

Fig. S8. FTIR spectra of NBC and pure BC membranes.

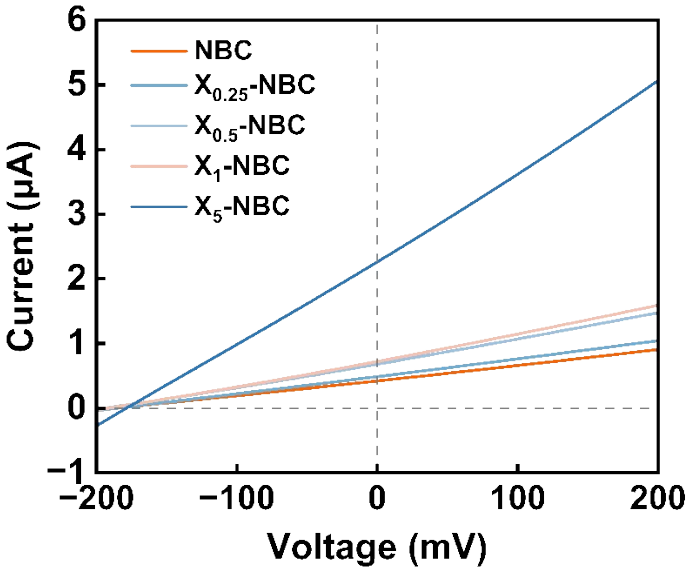

Fig. S9. *I-V* curves of NBC, $X_{0.25}$-NBC, $X_{0.5}$-NBC, X_1-NBC, X_5-NBC membranes under 1 mM/50 M KCl concentration gradient.

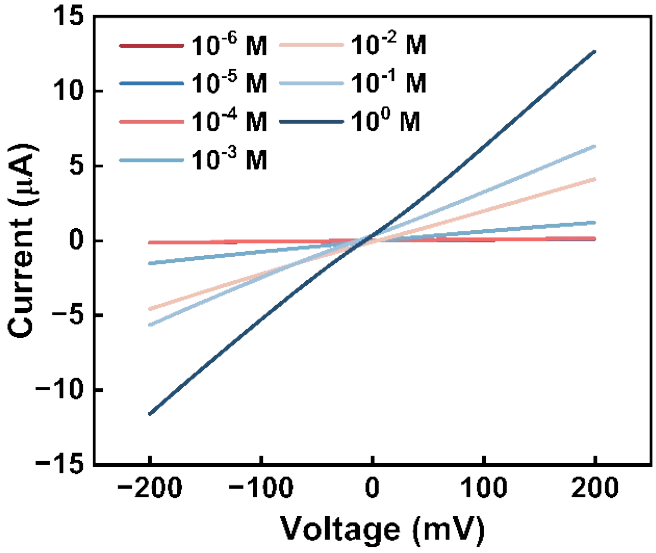

Fig. S10. *I-V* curves of X_5-NBC membrane at different KCl concentrations.

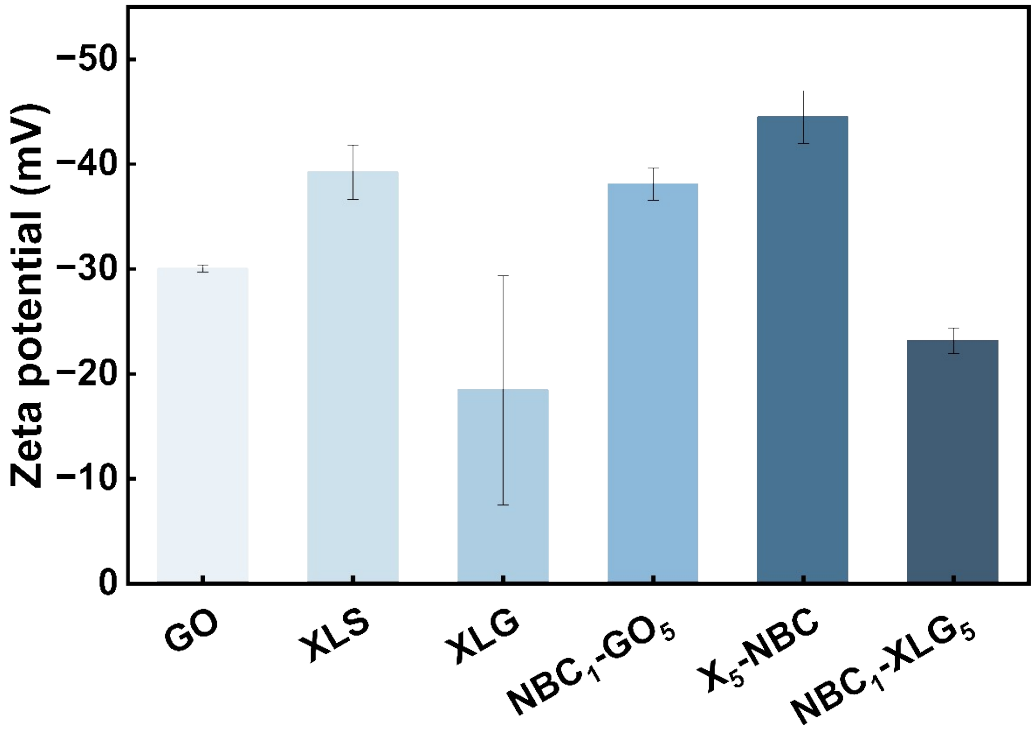

Fig. S11. Comparison of zeta potentials of GO, XLS, XLG aqueous dispersions and NBC_1-GO_5, X_5-NBC, and NBC_1-XLG_5 composite membranes.

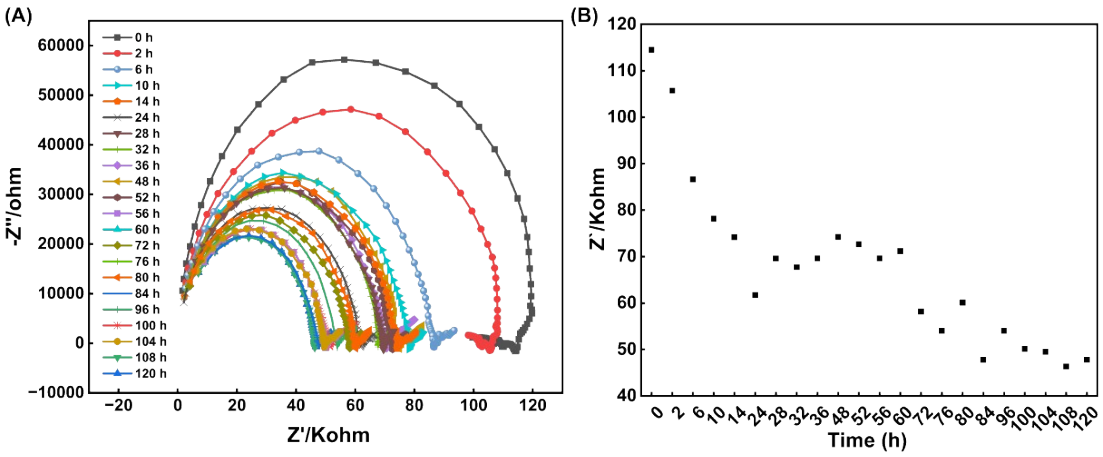

Fig. S12. (A) Nyquist plots of theX_5-NBC measured for a total duration of 120 h. (B) The relationship between real-part impedance (Z`) and time, highlighting the dynamic changes in internal resistance during the long-term test.

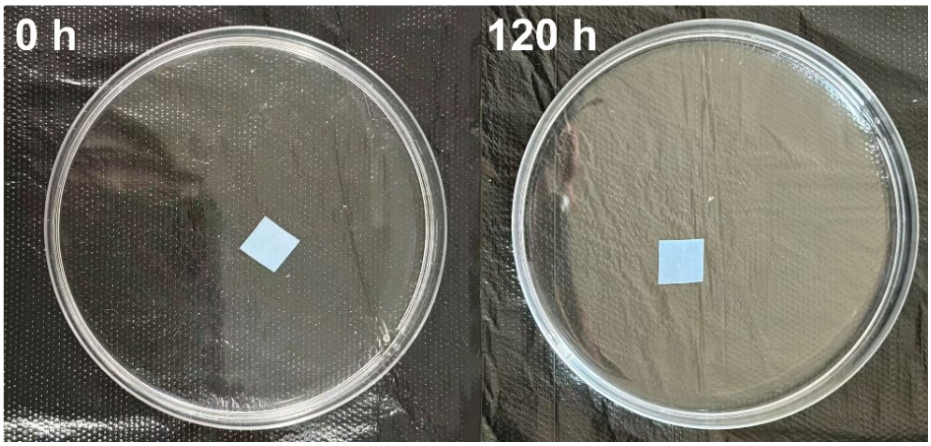

Fig. S13. Photograph of the X_5-NBC membrane retaining its complete structure after 120 h of immersion.

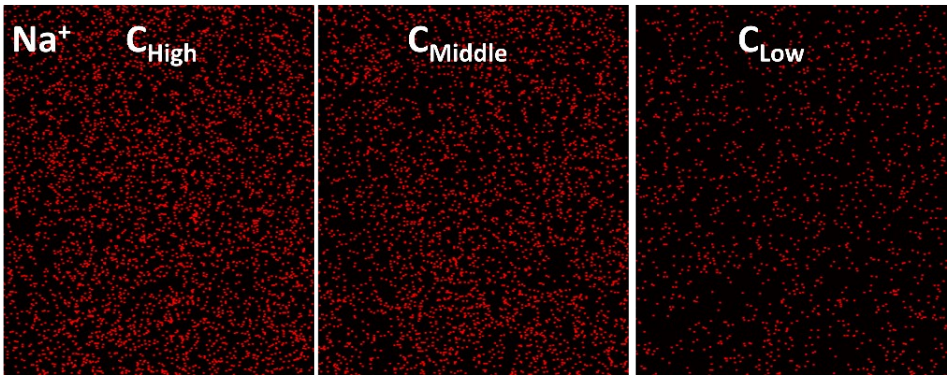

Fig. S14. Na^+ ionized EDS of X_5-NBC membrane after 120 h immersion under 50-fold concentration gradient.

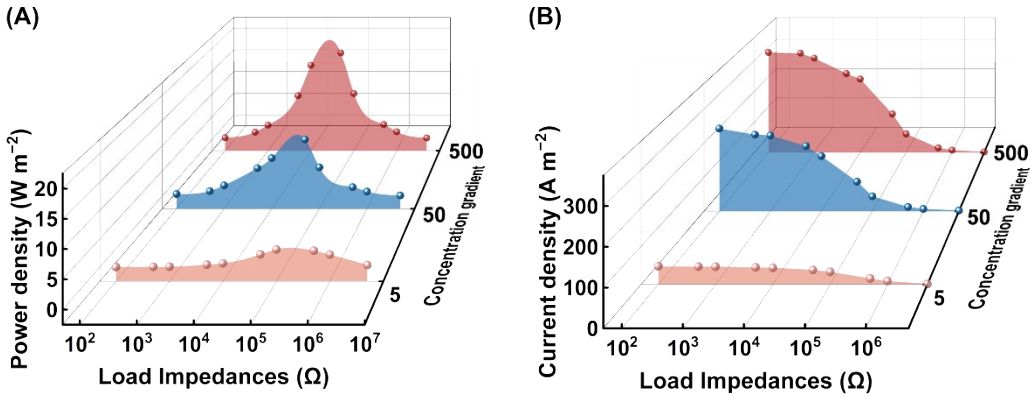

Fig. S15. Influence of salt concentration gradient on the (A) power density and (C) current density in X_5-NBC membrane.

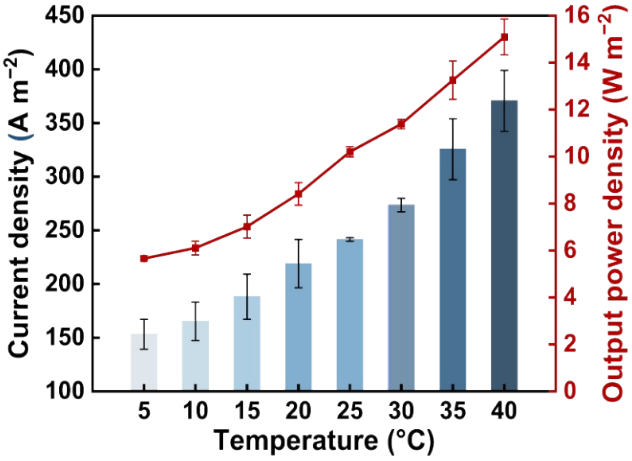

Fig. S16. Influence of the temperature on the output power density and current density in X_5-NBC membrane.

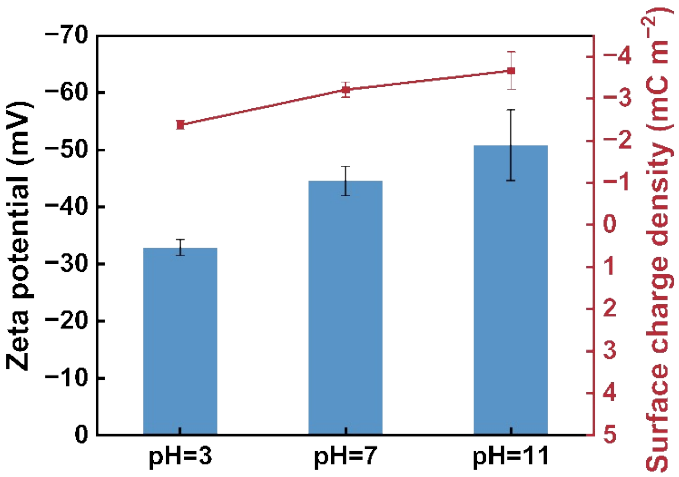

Fig. S17. Zeta potential and surface charge density of X_5-NBC membrane in different pH environments.

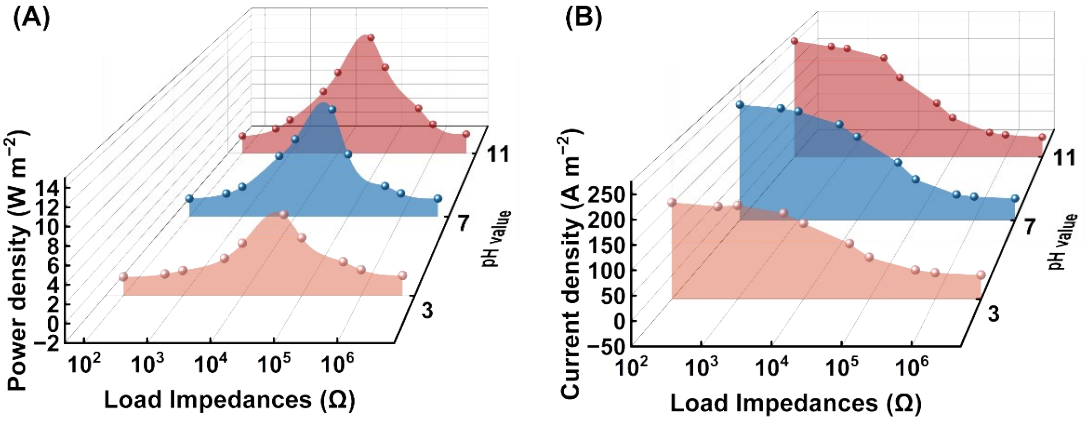

Fig. S18. Influence of pH on the (A) power density and (C) current density in X_5-NBC membrane.

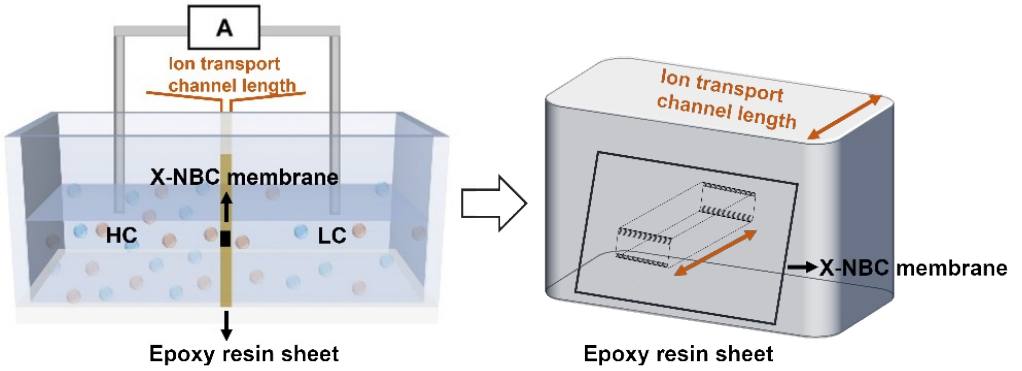

Fig. S19. Schematic diagram of ion transport channel length.

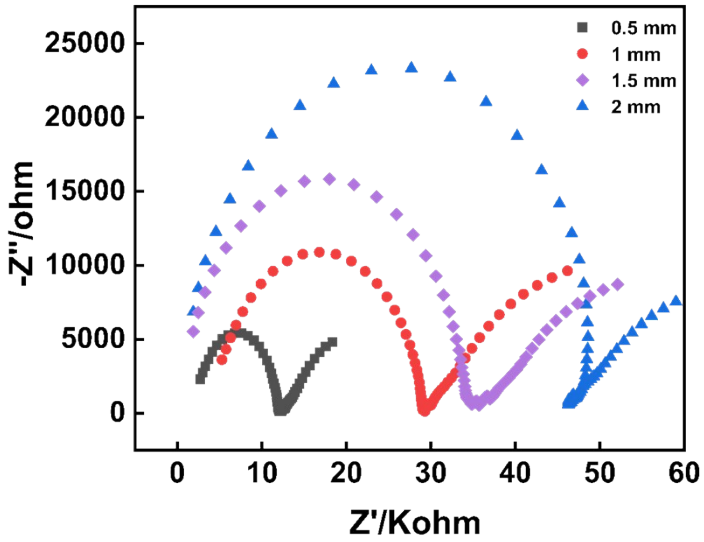

Fig. S20. Nyquist plots for different ion transport channel lengths.

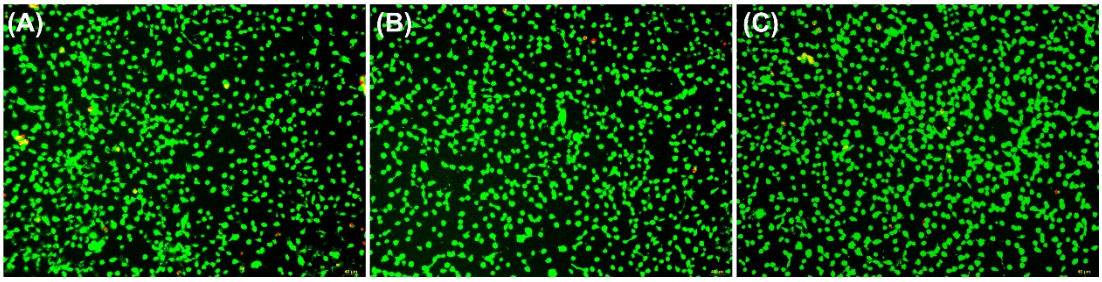

Fig. S21. Cytocompatibility fluorograms of X-NBC membranes. (A) $X_{0.25}$-NBC, (B) $X_{0.5}$-NBC and (C) X_1-NBC (Red color indicates dead cells, green color indicates live cells).

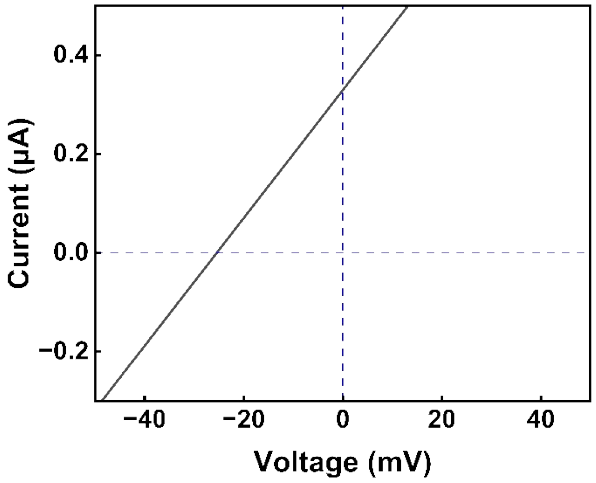

Fig. S22. I-V curves of X_5-NBC under artificial urine/PBS concentrations（artificial urine: NaCl: 128 mM, KCl: 60 mM, Urea: 303 mM, Na_3PO_4: 29 mM, Creatinine: 18 mM, Albumin: 0.75μM.）(PBS: KCl: 2.67 mM, NaCl: 137.93 mM，Na_2HPO_4: 8.07 mM, KH_2PO_4:1.47mM）

Table S1. Mass-balance verification of XLS incorporation in the X-NBC membrane series.

Sample	XLS Input (mg)	NBC input (mg)	Total input (mg)	Dry membrane weight (mg)	Retention (%)
XLS	100	0	100	0	0
$X_{0.25}$-NBC	5	20	25	25	100
$X_{0.5}$-NBC	10	20	30	30	100
X_1-NBC	20	20	40	39.9	99.75
X_5-NBC	100	20	120	119.8	99.92

Table S2. V_{OC}, E_{redox}, and E_{diff} of X_5-NBC membranes under different concentration gradients.

	5	50	500
V_{OC}/mV	93	178	227
E_{redox}/mV	37	89	112
E_{diff}/mV	56	89	115

Table S3. Donnan analysis of the geometric compensation effect in pure NBC and X_5-NBC.

Interface	c (mM)	X_V/c	Donnan exclusion
Dilute side	1	6.97	$t^+ \rightarrow 0.98$
Concentrated side	500	0.014	Negligible

Table S4. Donnan analysis of the geometric compensation effect in pure NBC and X_5-NBC.

Membrane	σ (mC m^{-2})	h (nm)	X_v (mM)	t^+ (at c_L = 1 mM)
Pure NBC	5.43	~150	0.75	0.68
X_5-NBC	3.36	~10	6.97	0.98

Table S5. Compare with the reported improvement of energy conversion performance by eliminating the ICP effect to enhance the permeability of heterojunctions.

Membranes	Power density (W m^{-2})	Testing area (mm^2)	Salt gradient	
SPC/T-CNF	0.73	0.03	0.01/0.5 M KCl	[4]
ILs/BC	0.7	0.785	0.01/0.5 M NaCl	[5]
HGO/CNF	1.25		0/01/0.5 M KCl	[6]
PSS/CNF	1.75	0.03	0/01/0.5 M KCl	[7]
MOF/T-CNF	1.87	0.02	0.01/0.5 M KCl	[8]

RCNFs	2.57	29.5	0.01/0.5 M NaCl	[9]
CNC/PVA@UiO-66	5.1	0.0043	0.01/0.5 M KCl	[10]
MXene/CNF	8.87	0.038	0.01/0.5 M NaCl	[11]
PCC	9	0.075	0.01/1 M NaCl	[12]
SPfs	8.3	0.03	0.01/0.5 M NaCl	[13]
RC-Fe3O4-NH2	4.9	0.03	0.01/0.5 M NaCl	[14]
(TOCNFs/MXene)$_3$	2.86	0.03	0.01/0.5 M NaCl	[15]
MXene/BNC	0.91	1	0.01/0.5 M NaCl	[16]
CNF-CNT/AAO	4.2	0.03	0.01/0.5 M NaCl	[17]
X_5-NBC	10.8 11.1 13.8 14.8	0.03	0.01M/0.5M NaCl	This work

References

1. T. Zhu, Y. Kong, B. Lyu, L. Cao, B. Shi, X. Wang, X. Pang, C. Fan, C. Yang, H. Wu and Z. Jiang, *Nat. Commun.*, 2023, **14**, 5926.
2. I. I. Ryzhkov, D. V. Lebedev, V. S. Solodovnichenko, A. V. Minakov and M. M. Simunin, *J. Membr. Sci.*, 2018, **549**, 616−630.
3. J. Gao, W. Guo, D. Feng, H. Wang, D. Zhao and L. Jiang, *Journal of the American Chemical Society*, 2014, **136**, 12265−12272.
4. Q. He, S. Qi, M. Ahmad, T. Zhang and S. Wang, *Int. J. Biol. Macromol.*, 2025, **296**, 139643.
5. X. Zhang, H. Huang, S. Chen, Y. Xu and F. Xu, *Int. J. Biol. Macromol.*, 2024, **258**, 128984.
6. S. Wang, Z. Shan, M. Ahmad, Z. Li and Z. Sun, *ACS Appl. Nano Mater.*, 2024, **7**, 14265−14274.
7. Z. Li, J. Zhang, M. Ahmad, Z. Sun, W. Fu and S. Wang, *ACS Appl. Polym. Mater.*, 2024, **6**, 1439−1448.
8. W. Fu, J. Zhang, Q. Zhang, M. Ahmad, Z. Sun, Z. Li, Y. Zhu, Y. Zhou and S. Wang, *Int. J. Biol. Macromol.*, 2024, **257**, 128546.
9. B. Zhou, J. Zou, Z. Lin, Z. Yuan, X. Qin, P. Chen and D. Ye, *Chem. Eng. J.*, 2023, **457**, 141167.
10. X. Wang, M. Li, Y. Xiong, H. Qin, Q. Li, F. Zhang, Y.-L. Yu and G. Qing, *Small*, 2025, **21**, 2408695.
11. Z. Yuan, B. Zhou, K. Yuan, Z. Xie, K. Zheng, H. Wang, C. Jiao and D. Ye, *Nano Energy*, 2024, **124**, 109450.
12. J. Shi, K. Lin, Y. Liu, S. Niu, Y. Zhang, W. Yang, L. Huang, J. Li and L. Chen, *Chem. Eng. J.*, 2024, **495**, 153496.
13. S. Hou, J. Zhao, Z. Zhang, Y. Hu, L. Fu, Y. Qian, W. Chen, S. Zhou, X. Kong and L. Wen, *Sci. China Mater.*, 2024, **67**, 2567−2574.
14. X. Li, P. Cheng, J. Zhang, H. Nawaz, Y. Xu and F. Xu, *Carbohydr. Polym.*, 2022, **292**, 119657.
15. X. Li, J. He, B. Lu and J. Zhai, *Chem. Eng. J.*, 2024, **493**, 152375.
16. Y. Xu, K. Zhang, S. Chen, X. Zhang, Y. Chen, D. Li and F. Xu, *Electrochim. Acta*, 2022, **412**, 140162.
17. A. Awati, S. Zhou, T. Shi, J. Zeng, R. Yang, Y. He, X. Zhang, H. Zeng, D. Zhu, T. Cao, L. Xie, M. Liu and B. Kong, *ACS Appl. Mater. Interfaces*, 2023, **15**, 27075−27088.